ChemComm

COMMUNICATION

Mechanochemical Synthesis of 0D and 3D Cesium Lead Mixed Halide Perovskites†

Received 00th January 20xx,
Accepted 00th January 20xx

DOI: 10.1039/x0xx00000x

www.rsc.org/

Abhoy Karmakar, Mya S. Dodd, Xiaoyue Zhang, Meagan S. Oakley, Mariusz Klobukowski and Vladimir K. Michaelis*

A simplified mechanochemical synthesis approach for Cs-containing mixed halide perovskite materials of lower and higher dimensionality (0D and 3D, respectively) is presented with stoichiometric control from their halide salts, CsX and PbX_2 (X = Cl, Br, I). Excellent optical bandgap tunability through halide substitution is supported by property measurements and changes to the materials structure. Complementary NMR and XRD methods, along with support from DFT calculations, reveal highly crystalline 0D and 3D solid solutions with a complex arrangement of $[PbX_{6-x}X'_x]^{4-}$ pseudooctahedra caused by halide distribution about the Pb centre.

Lead halide perovskite (LHP) materials have demonstrated an impressive increase in photoconversion efficiency (PCE) over the past decade, with hybrid organic-inorganic LHP materials exhibiting ca. 22% PCE in perovskite solar-cell (PSC) technologies.[1] Although methylammonium (MA) and formamidinium (FA) LHPs ($APbX_3$, where A = MA or FA and X = Cl^-, Br^-, and I^-) are commonly used as the active layer in PSCs, the use of Cs-based LHPs ($CsPbX_3$) is rapidly gaining interest due to their robustness, including high thermal (non-volatile) and moisture stability[2–4], and attractive optoelectronic properties[4–8]. For example, Cs-based LHPs have achieved ca. 20% PCEs[9] and provide easy to control bandgap tailorability and enhanced stability through manipulation of the halide composition (mixed-halide perovskites, MHPs) - critical features when engineering light emitting diode materials[4,6–8,10] and a promising green technology for innovative photovoltaic smart windows[11].

Predominantly, LHPs are synthesized using either solvent-synthesis or gas-phase deposition techniques[12–14], however mechanochemical synthesis (MCS) has emerged as an attractive alternative which provides a stoichiometric method to prepare bulk micro- and nanocrystalline hybrid and non-hybrid LHP materials without the need for solvents, ultimately avoiding many hazards.[15–24] Moreover, LHPs prepared via MCS exhibit enhanced material properties and device performance when compared to those prepared using traditional solvent-synthesis approaches.[21] This highlights the growing interest in MCS as it is an effective synthetic approach here and in other advanced functional materials.[25]

Recently, low-dimensional LHPs such as 0D LHPs have been gaining interest due to their improved stability and enhanced photoluminescent properties as compared to 3D LHPs.[26–29] 3D and 0D LHPs can be expressed using the general formula ABX_3 and A_4BX_6, respectively (where, A = Cs^+, B = Pb^{2+} and X = Cl^-, Br^-, I^-). In the process of reducing the 3D structure to a 0D perovskite, structural features are impacted such that the $[PbX_{6-x}X'_x]^{4-}$ octahedra alter the connectivity, from corner sharing (3D) to isolated tilted-unit 0D LHPs (Scheme 1).

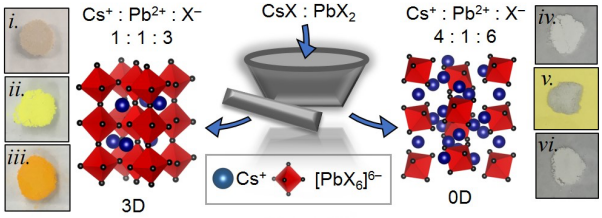

Scheme 1. Preparation of 3D and 0D parent and MHPs starting with CsX and PbX_2 salts by the MCS approach. The dimensionality of the final product depends on the molar ratios of Cs^+, Pb^{2+} and X^- compositions. Photos of 3D (i. $CsPbCl_3$, ii. $CsPbCl_{1.5}Br_{1.5}$, and iii. $CsPbBr_3$) and 0D (iv. Cs_4PbCl_6, v. $Cs_4PbCl_3Br_3$, and vi. Cs_4PbBr_6) parents and their 1: 1 MHP prepared by MCS.

The interconnectivity between structure and optical properties warrants a careful analysis of the unique 3D and 0D features. We turn our attention to the 3D parent, $CsPbX_3$, and the MHPs ($CsPbCl_xBr_{3-x}$ and $CsPbBr_xI_{3-x}$; $0 < x < 3$), all prepared by MCS initiated from CsX and PbX_2 salts (see the ESI†). For the Cl/Br $CsPbCl_xBr_{3-x}$ MHPs, an expected phase-pure perovskite material was easily obtained by MCS and confirmed through powder X-ray diffraction (XRD) data (Fig. S1a). The Br/I series

Department of Chemistry, University of Alberta, Edmonton, Alberta, T6G 2G2, Canada. E-mail: vladimir.michaelis@ualberta.ca

† Electronic supplementary information (ESI) available: Experimental section, Table S1-S2 and Figures S1-S10. See DOI:

Please do not adjust margins

($CsPbBr_xI_{3-x}$ MHPs and $CsPbI_3$) were more challenging, requiring an additional thermal annealing step post-MCS to obtain phase-pure perovskite phases (Fig. S1b).[30,31] All three phase-pure parent perovskites are orthorhombic (space group *Pnma* or *Pnam*) at room temperature.[32–34] Substituting chloride, radius, r(Cl^-) = 167 pm, with the larger bromide , r(Br^-) = 182 pm, (or Br^- with I^- (r(I^-) = 206 pm))[35] causes a shift towards lower 2θ values in the XRD pattern (Fig. 1a and S1) which is attributed to an increase in the average unit cell parameters.[22,23] The halide composition in MHPs also alters the colour of the bulk materials (Scheme 1 and Fig. S2a), suggesting a change in bandgap. Fig. 1b also shows the UV-Vis absorbance spectra of the three $CsPbX_3$ parent perovskites, along with their 1:1 MHPs, namely, $CsPbCl_{1.5}Br_{1.5}$ and $CsPbBr_{1.5}I_{1.5}$. Absorbance data for each MHP, obtained using the Kubelka-Munk transformation (see the ESI†) from the DR measurements, are shown in Fig. S2. This data indicates that the direct bandgaps vary linearly from 2.94 to 2.32 ($CsPbCl_xBr_{3-x}$ MHPs, Fig. S2d) and from 2.32 to 1.72 eV ($CsPbBr_xI_{3-x}$ MHPs, Fig. S2e) upon halide substitution.

The XRD and UV-Vis absorbance spectra inform about the long-range crystallinity and bandgap properties, respectively; to evaluate the local Pb chemical environments, another spectroscopy method is required, namely NMR spectroscopy. We and others have shown this method to be an extremely sensitive analytical tool to structurally probe A- and B-site environments within halide perovskite materials.[20,22–24,36–41] The large ^{207}Pb chemical shift range (~20,000 ppm) makes ^{207}Pb NMR highly sensitive to the local chemical structure, making it well suited to evaluate MHPs. Lead is coordinated to six halides forming pseudooctahedra. Depending on halogen arrangement a total of ten distinguishable isomers are possible (Table S2). Fig. 1c shows the ^{207}Pb NMR spectra of the non-spinning $CsPbX_3$ parent perovskites and of two MHPs, $CsPbCl_{1.5}Br_{1.5}$ and $CsPbBr_{1.5}I_{1.5}$ (see Fig. S3 for MHPs). The ^{207}Pb NMR chemical shifts (peak maxima, $\delta_{cs}(^{207}Pb)$) for the $CsPbX_3$ parent perovskites show Gaussian-like line shapes that shift to higher frequency from $\delta_{cs}(^{207}Pb)$ = −728 ± 1 ppm ($CsPbCl_3$) to 1265 ± 20 ppm (γ-$CsPbI_3$), spanning nearly 2,000 ppm (Fig. 1c and Table S1), similar to MA- and FA-based LHPs.[22,23] The ^{207}Pb NMR linewidths for $CsPbX_3$ parent materials increase systematically upon X-site substitution from Cl to Br to I with a full-width at half-maximum (fwhm) of ca. 5, 18 and 25 kHz, respectively (B_0 = 11.75 T). The broad ^{207}Pb NMR line widths are mainly due to the direct and indirect spin-spin coupling between Pb and six quadrupolar nuclei (I = 3/2 for $^{35/37}$Cl or $^{79/81}$Br, and I = 5/2 for ^{127}I) in $[PbX_6]^{4-}$.[22,23,37] An asymmetric ^{207}Pb NMR line shape is observed for the non-perovskite, δ-$CsPbI_3$, due to a sizable magnetic shielding anisotropy with an isotropic chemical shift, $\delta_{iso}(^{207}Pb)$ = 1065 ± 30 ppm, span (Ω) = 650 ± 30 ppm, and skew (κ) = 0.7 ± 0.1. As for $FAPbI_3$,[23] $\delta_{cs}(^{207}Pb)$ for the perovskite-phase, γ-$CsPbI_3$, is shifted towards higher frequency compared to that for δ-$CsPbI_3$ (Fig. S4a). The ^{207}Pb NMR spectra for the MHPs indicate multiple Pb sites (Fig. 1c, S3 and S5) due to distinct local $[PbX_{6-x}X'_x]^{4-}$ chemical environments, a conclusion that is supported by quantum chemical calculations (vide infra). These findings are consistent with those for MA- and FA-based hybrid MHPs studied previously, revealing solid-solution behaviour.[22,23]

Cs_4PbX_6 (X = Cl, Br) parent 0D LHPs and the $Cs_4PbCl_3Br_3$ MHP were also prepared by MCS starting with their respective salts (see the ESI†); XRD (Fig. 1e) indicate these materials adopt a trigonal space group $R\bar{3}c$.[42] Unlike the 3D materials, the colour of 0D LHPs is independent of halide substitution, appearing as colourless white solids (Scheme 1). For example, 3D $CsPbBr_3$ is an orange solid whereas the corresponding 0D Cs_4PbBr_6 is a white material. The change in colour is due to the loss of strong orbital overlap of the $[PbX_{6-x}X'_x]^{4-}$ cluster connectivity in 0D material and indicative of wider bandgaps.[28] The UV-vis absorption spectra (Fig. 1f) confirm that all 0D LHPs absorb in the UV-region and show a single molecule-like excitonic absorption band. Furthermore, the direct bandgap for 0D LHPs alters upon halide substitution increasing with Cl content (3.75 (Cs_4PbBr_6), 3.85 ($Cs_4PbCl_3Br_3$) and 4.07 eV (Cs_4PbCl_6)). The UV-vis spectra for the 0D materials do not show any absorption between 2.2 and 3.5 eV (Fig. 1f); suggesting the absence of nanocrystal-like 3D $CsPbX_3$ impurities, further supported by ^{133}Cs MAS NMR (vide infra).[28]

The ^{207}Pb NMR chemical shifts for the 0D parent perovskites are $\delta_{cs}(^{207}Pb)$ = −1139 ± 1 ppm (Cs_4PbCl_6) and −385 ± 5 ppm (Cs_4PbBr_6), Fig. 1g. The main difference between the 3D and 0D LHPs is the $[PbX_{6-x}X'_x]^{4-}$ connectivity as discussed earlier (Scheme 1). The Pb chemical environments are sensitive to this change in crystal structure shifting the $\delta_{cs}(^{207}Pb)$ to lower frequency for the 0D LHPs as compared to that for the 3D materials (e.g., $\delta_{cs}(^{207}Pb)$ = −728 (3D) vs. −1139

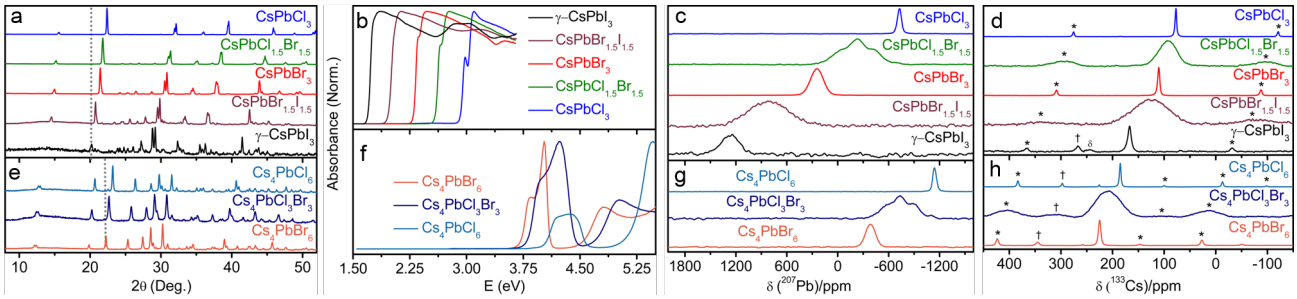

Fig. 1. Room temperature powder XRD patterns (a, e), UV-Vis normalized absorbance spectra (b, f), solid-state ^{207}Pb NMR spectra under non-spinning sample conditions at 11.75 T (c, g), and ^{133}Cs NMR spectra with a magic-angle spinning (MAS) frequency of 13 kHz at 11.75 T (d, h) of 3D $CsPbX_3$ and 0D Cs_4PbX_6 perovskites, respectively, as indicated. The dotted lines in (a) and (e) are the guide for the eye. The asterisks (*), dagger (†) and delta (δ) in (d) and (h) indicate spinning sidebands, an unidentified Cs-containing impurity and δ-$CsPbI_3$, respectively.

ppm (0D)). The ^{207}Pb NMR spectrum of the Cl/Br MHP 0D material displays a Gaussian-like distribution of unique Pb chemical environments that shift to higher frequency with Br incorporation, mirroring the behaviour seen in the 3D materials. The XRD and NMR features indicate that solid solution-like compositions are readily formed using the solvent-free MCS approach. The different ^{207}Pb NMR chemical shifts for the 3D and 0D compositions indicate that these appear to be sensitive to both local $[PbX_{6-x}X'_x]^{4-}$ polyhedra and the crystal structure. Density functional theory (DFT) was used to calculate NMR chemical shieldings of $[PbX_{6-x}X'_x]^{4-}$ anionic clusters modeled from their 3D and 0D crystalline structures and the results correlate well with experimentally determined chemical shifts. The calculations show sizeable chemical shielding anisotropies, consistent with the non-cubic nature of the Cs-based LHP space groups, which could further complicate the ^{207}Pb NMR line shapes.

Fig. 2 shows excellent agreement between the experimental and calculated ^{207}Pb NMR chemical shifts for Cl/Br mixtures for 3D perovskites. Although the 0D clusters correctly predict the linear trend, the shifts are overestimated. A larger anionic model may be needed to capture the long-range effects, but at significant computational cost. The overall trend to higher chemical shift with Br incorporation, as well as the different chemical shifts between the parent compounds from the 3D vs 0D structures found experimentally with ^{207}Pb NMR are reflected in the calculated results (see the ESI†).

The A-site is surrounded by 12 halides in a pseudo-cuboctahedral environment for 3D LHPs. Since ^{133}Cs is highly receptive (100% n.a.), ^{133}Cs NMR can provide complementary information to that obtained via ^{207}Pb NMR. Fig. 1d and 1h show ^{133}Cs NMR spectra for the 3D and 0D materials, respectively. Fig. 1d shows the three $CsPbX_3$ parents and two MHPs, $CsPbCl_{1.5}Br_{1.5}$ and $CsPbBr_{1.5}I_{1.5}$. The parent compounds show sharp Gaussian-like resonances with $\delta_{iso}(^{133}Cs)$ = 76.9, 110.3 and 166.9 ppm for $CsPbCl_3$, $CsPbBr_3$ and γ-$CsPbI_3$, respectively. The $\delta_{iso}(^{133}Cs)$ values for the MHPs are between those for their parent compounds, with a linear relationship with halide compositions (Fig. 1d and S6). Unlike the ^{207}Pb NMR spectra, the ^{133}Cs NMR spectra for the MHPs display a single broad Gaussian-like resonance. Although ^{133}Cs is a quadrupolar nucleus (I = 7/2), the broadening is not caused by a sizeable quadrupole interaction, but from a distribution of chemical shifts (consistent with a high degree of random halide arrangement). The ^{133}Cs nucleus is highly sensitive to small changes in its local coordination environment (i.e., highly polarizable) with a moderately large chemical shift range. For example, the ^{133}Cs NMR linewidth for $CsPbCl_{1.5}Br_{1.5}$ is 2 kHz as compared to 0.2 kHz for the $CsPbBr_3$ parent (B_0 = 11.75 T). Unlike the corresponding ^{207}Pb NMR results, the ^{133}Cs NMR chemical shift for δ-$CsPbI_3$ (247.0 ppm) is greater than that for γ-$CsPbI_3$ (166.9 ppm), though they have comparable ^{133}Cs NMR lineshapes and linewidths (Fig. S4b and Table S1). Similar spectral features are apparent for the 0D perovskites (Fig. 1h). Most interestingly, ^{133}Cs NMR confirms the absence of other stable ternary cesium lead halide compounds such as 3D $CsPbX_3$ or 2D $CsPb_2X_5$ impurities in our 0D materials (Fig. S7). This result suggests MCS is a suitable synthetic approach to avoid nanocrystal-like 3D $CsPbX_3$ impurities in 0D materials.[28]

At room temperature the γ-$CsPbI_3$ perovskite phase is unstable, rapidly converting to the more energetically favourable non-perovskite δ-$CsPbI_3$ phase under ambient conditions, in line with previous DFT results.[34] In situ kinetic measurements are possible due to the high resolution and sensitivity of ^{133}Cs NMR, enabling further study into the phase conversion mechanism from γ- to δ-$CsPbI_3$ using time-dependent measurements. Probing this transformation (Fig. S8) indicates that the process follows first-order kinetics, whereby a half-life of 29 ± 2 minutes for the phase conversion is determined. This explains the difficulty in handling this material and provides a measure for comparison for future chemical modifications that may delay this phase change.

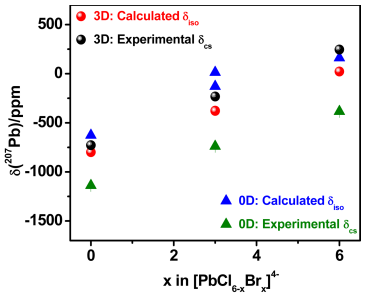

Fig. 2. The ^{207}Pb NMR chemical shifts calculated with DFT for a $[PbCl_{6-x}Br_x]^{4-}$ anionic 0D and 3D models.

Hybrid lead halide perovskites have demonstrated organic (A-site) and halide (X-site) dynamics within semiconducting solids that may be a vital component for effective charge separation, lifetime and collection.[22,23,37,38,43] We have shown previously[22,23] that ^{207}Pb EXSY NMR is an effective approach to demonstrate halide exchange within MA- and FA-MHPs and was attempted for the 0D and 3D Cl/Br MHPs ($CsPbCl_{1.5}Br_{1.5}$ and $Cs_4PbCl_3Br_3$). Mixing times were varied up to 50 ms; no cross-peaks were detected on these time scales (Fig. S9). These findings suggest that there is no significant halide exchange for these materials. It is of interest to point out that the tilted lattice (3D), or isolated octahedron (0D), present in Cs-MHPs may form localized inhomogeneous domains, which could suppress rapid halide exchange, while Cs^+ has the largest charge density (field strength) when compared to MA^+ and FA^+, which may further complicate halide dynamics, clearly an area requiring further study.

In summary, Cs-MHPs are readily synthesized from their salts using a MCS approach. This facilitates solvent-free synthesis, delivering stoichiometric bulk solid-solutions with exceptional bandgap tunability from 1.72 to 2.94 eV (3D) and 3.75 to 4.07 eV (0D). Although the luminescence properties of these 0D LHPs requires further study, their wide bandgap may be attractive for high energy UV-luminescence properties. The 0D and 3D LHP parent and MHPs display unique ^{207}Pb and ^{133}Cs NMR signatures with a Gaussian-like distribution of $[PbX_{6-x}X'_x]^{4-}$ polyhedra due to the random halide arrangements. The calculated results support conclusions based on experimental ^{207}Pb NMR signatures. The EXSY data did not reveal halide exchange, which is a unique feature to the Cs-containing LHPs.

Tuning the kinetics of the phase conversion from γ- to δ-$CsPbI_3$ may prove useful for future sensor and optoelectronic applications.

This work is supported by NSERC (DG and CREATE-ATUMS), Future Energy Systems (CFREF), CFI and the Government of Alberta. A.K. is supported by an Alberta Innovates Graduate Student Scholarship. M.S.D. and X.Z. were partially supported by ECO-Canada and UARE, respectively. M.S.O was supported by the Queen Elizabeth II Doctoral Grant. Access to the 21.1 T NMR spectrometer was provided by the National Ultrahigh-Field NMR Facility for Solids (http://nmr900.ca). Dr. Victor Terskikh is thanked for scientific discussion and 21.1 T assistance.

Conflicts of interest

There are no conflicts to declare.

Notes and references

1 M. A. Green, Y. Hishikawa, E. D. Dunlop, D. H. Levi, J. Hohl-Ebinger and A. W. Y. Ho-Baillie, *Prog. Photovoltaics Res. Appl.*, 2018, **26**, 3–12.
2 R. J. Sutton, G. E. Eperon, L. Miranda, E. S. Parrott, B. A. Kamino, J. B. Patel, M. T. Hörantner, M. B. Johnston, A. A. Haghighirad, D. T. Moore and H. J. Snaith, *Adv. Energy Mater.*, 2016, **6**, 1502458.
3 C. C. Stoumpos and M. G. Kanatzidis, *Adv. Mater.*, 2016, **28**, 5778–5793.
4 J. S. Manser, J. A. Christians and P. V. Kamat, *Chem. Rev.*, 2016, **116**, 12956–13008.
5 G. Rainò, M. A. Becker, M. I. Bodnarchuk, R. F. Mahrt, M. V. Kovalenko and T. Stöferle, *Nature*, 2018, **563**, 671–675.
6 L. Protesescu, S. Yakunin, M. I. Bodnarchuk, F. Krieg, R. Caputo, C. H. Hendon, R. X. Yang, A. Walsh and M. V. Kovalenko, *Nano Lett.*, 2015, **15**, 3692–3696.
7 Y. Wei, Z. Cheng and J. Lin, *Chem. Soc. Rev.*, 2018, **48**, 310–350.
8 K. Chen, S. Schunemann, S. Songb and H. Tuysuz, *Chem. Soc. Rev.*, 2018, **47**, 7045–7077.
9 J. Liang, Z. Liu, L. Qiu, Z. Hawash, L. Meng, Z. Wu, Y. Jiang, L. K. Ono and Y. Qi, *Adv. Energy Mater.*, 2018, **8**, 1–7.
10 X. Li, Y. Wu, S. Zhang, B. Cai, Y. Gu, J. Song and H. Zeng, *Adv. Funct. Mater.*, 2016, **26**, 2435–2445.
11 J. Lin, M. Lai, L. Dou, C. S. Kley, H. Chen, F. Peng, J. Sun, D. Lu, S. A. Hawks, C. Xie, F. Cui, A. P. Alivisatos, D. T. Limmer and P. Yang, *Nat. Mater.*, 2018, **17**, 261–267.
12 M. Liu, M. B. Johnston and H. J. Snaith, *Nature*, 2013, **501**, 395–398.
13 Y. Zhao and K. Zhu, *Chem. Soc. Rev.*, 2016, **45**, 655–689.
14 W. A. Dunlap-shohl, Y. Zhou, N. P. Padture and D. B. Mitzi, *Chem. Rev.*, 2019, **119**, 3193–3295.
15 O. Y. Posudievsky, N. V Konoshchuk, V. L. Karbivskyy, O. P. Boiko, V. G. Koshechko and V. D. Pokhodenko, *Theor. Exp. Chem.*, 2017, **53**, 223–230.
16 Y. El Ajjouri, V. S. Chirvony and M. Sessolo, *RSC Adv.*, 2018, **8**, 41548–41551.
17 Y. El Ajjouri, F. Palazon, M. Sessolo and H. J. Bolink, *Chem. Mater.*, 2018, **30**, 7423–7427.
18 L. Protesescu, S. Yakunin, O. Nazarenko, D. N. Dirin and M. V Kovalenko, *ACS Appl. Mater. Interfaces*, 2018, **1**, 1300−1308.
19 P. Pal, S. Saha, A. Banik, A. Sarkar and K. Biswas, *Chem. - A Eur. J.*, 2018, **24**, 1811–1815.
20 D. Prochowicz, P. Yadav, M. Saliba, D. J. Kubicki, M. M. Tavakoli, S. M. Zakeeruddin, J. Lewiński, L. Emsley and M. Grätzel, *Nano Energy*, 2018, **49**, 523–528.
21 D. Prochowicz, M. Franckevicius, A. M. Cieslak, S. M. Zakeeruddin, M. Graatzel and J. Lewinski, *J. Mater. Chem. A*, 2015, **3**, 20772–20777.
22 A. Karmakar, A. M. Askar, G. M. Bernard, V. V. Terskikh, M. Ha, S. Patel, K. Shankar and V. K. Michaelis, *Chem. Mater.*, 2018, **30**, 2309–2321.
23 A. M. Askar, A. Karmakar, G. M. Bernard, M. Ha, V. V. Terskikh, B. D. Wiltshire, S. Patel, J. Fleet, K. Shankar and V. K. Michaelis, *J. Phys. Chem. Lett.*, 2018, **9**, 2671–2677.
24 D. J. Kubicki, D. Prochowicz, A. Hofstetter, S. M. Zakeeruddin, M. Grätzel and L. Emsley, *J. Am. Chem. Soc.*, 2017, **139**, 14173–14180.
25 S. L. James, C. J. Adams, C. Bolm, D. Braga, P. Collier, T. Friscic, F. Grepioni, K. D. M. Harris, G. Hyett, W. Jones, A. Krebs, J. Mack, L. Maini, A. G. Orpen, I. P. Parkin, W. C. Shearouse, J. W. Steed and D. C. Waddell, *Chem. Soc. Rev.*, 2012, **41**, 413–447.
26 M. I. Saidaminov, J. Almutlaq, S. Sarmah, I. Dursun, A. A. Zhumekenov, R. Begum, J. Pan, N. Cho, O. F. Mohammed and O. M. Bakr, *ACS Energy Lett.*, 2016, **1**, 840–845.
27 M. I. Saidaminov, O. F. Mohammed and O. M. Bakr, *ACS Energy Lett.*, 2017, **2**, 889−896.
28 Q. A. Akkerman, A. L. Abdelhady and L. Manna, *J. Phys. Chem. Lett.*, 2018, **9**, 2326–2337.
29 J. Almutlaq, J. Yin, O. F. Mohammed and O. M. Bakr, *J. Phys. Chem. Lett.*, 2018, **9**, 4131−4138.
30 C. C. Stoumpos, C. D. Malliakas and M. G. Kanatzidis, *Inorg. Chem.*, 2013, **52**, 9019−9038.
31 F. Hao, C. C. Stoumpos, D. H. Cao, R. P. H. Chang and M. G. Kanatzidis, *Nat. Photonics*, 2014, **8**, 489–494.
32 M. R. Linaburg, E. T. McClure, J. D. Majher and P. M. Woodward, *Chem. Mater.*, 2017, **29**, 3507–3514.
33 C. C. Stoumpos, C. D. Malliakas, J. A. Peters, Z. Liu, M. Sebastian, J. Im, T. C. Chasapis, A. C. Wibowo, D. Y. Chung, A. J. Freeman, B. W. Wessels and M. G. Kanatzidis, *Cryst. Growth Des.*, 2013, **13**, 2722−2727.
34 R. J. Sutton, M. R. Filip, A. A. Haghighirad, N. Sakai, B. Wenger, F. Giustino and H. J. Snaith, *ACS Energy Lett.*, 2018, **3**, 1787–1794.
35 R. D. Shannon, *Acta Cryst.*, 1976, **A32**, 751–767.
36 B. A. Rosales, L. Men, S. D. Cady, M. P. Hanrahan, A. J. Rossini and J. Vela, *Chem. Mater.*, 2016, **28**, 6848–6859.
37 G. M. Bernard, R. E. Wasylishen, C. I. Ratcliffe, V. Terskikh, Q. Wu, J. M. Buriak and T. Hauger, *J. Phys. Chem. A*, 2018, **122**, 1560–1573.
38 A. Senocrate, I. Moudrakovski, G. Y. Kim, T. Yang, G. Gregori, M. Grätzel and J. Maier, *Angew. Chem. Int. Ed.*, 2017, **56**, 7755–7759.
39 A. Senocrate, I. Moudrakovski, T. Acartuerk, R. Merkle, G. Y. Kim, U. Starke, M. Grätzel and J. Maier, *J. Phys. Chem. C*, 2018, **122**, 21803−21806.
40 A. Karmakar, M. S. Dodd, S. Agnihotri, E. Ravera and V. K. Michaelis, *Chem. Mater.*, 2018, **30**, 8280–8290.
41 A. M. Askar, G. M. Bernard, B. Wiltshire, K. Shankar and V. K. Michaelis, *J. Phys. Chem. C*, 2017, **121**, 1013–1024.
42 M. De Bastiani, I. Dursun, Y. Zhang, B. A. Alshankiti, X. H. Miao, J. Yin, E. Yengel, E. Alarousu, B. Turedi, J. M. Almutlaq, M. I. Saidaminov, S. Mitra, I. Gereige, A. Alsaggaf, Y. Zhu, Y. Han, I. S. Roqan, J. L. Bredas, O. F. Mohammed and O. M. Bakr, *Chem. Mater.*, 2017, **29**, 7108–7113.
43 W. M. J. Franssen, S. G. D. Van Es, R. Dervişoğlu, G. A. De Wijs and A. P. M. Kentgens, *J. Phys. Chem. Lett.*, 2017, **8**, 61–66.

TOC Graphic:

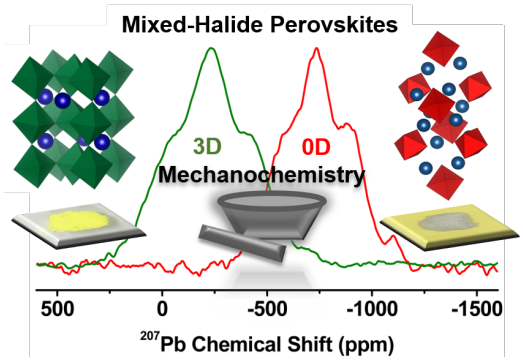
Mixed-Halide Perovskites
3D
0D
Mechanochemistry
500
0
-500
-1000
-1500
207Pb Chemical Shift (ppm)